Liver Steatosis Categorization on Contrast-Enhanced CT Using a Fully Automated Deep Learning Volumetric Segmentation Tool: Evaluation in 1204 Healthy Adults Using Unenhanced CT as a Reference Standard

Perry J. Pickhardt, MD[1], Glen M. Blake, PhD[2], Peter M. Graffy, BA[1], Veit Sandfort, MD[3], Daniel C. Elton, PhD[3], Alberto A. Perez, BE[1], Ronald M. Summers, MD, PhD[3]

Gastrointestinal Imaging · Original Research

Keywords

artificial intelligence, CT, deep learning, NAFLD, steatosis

Submitted: Jul 21, 2020
Revision requested: Aug 3, 2020
Revision received: Aug 10, 2020
Accepted: Aug 25, 2020
First published online: Sep 16, 2020

P. J. Pickhardt serves as an advisor to Bracco Diagnostics and Zebra Medical Vision and is a shareholder in SHINE, Elucent, and Cellectar. R. M. Summers receives royalties from iCAD, PingAn, Philips Healthcare, ScanMed, and Translation Holdings and research support from PingAn and Nvidia (graphics processing unit card donations). The remaining authors declare that they have no disclosures relevant to the subject matter of this article.

Supported in part by the Intramural Research Program of the National Institutes of Health (NIH) Clinical Center and conducted using the high performance computing capabilities of the NIH Biowulf cluster.

BACKGROUND. Hepatic attenuation at unenhanced CT is linearly correlated with the MRI proton density fat fraction (PDFF). Liver fat quantification at contrast-enhanced CT is more challenging.

OBJECTIVE. The purpose of this article is to evaluate liver steatosis categorization on contrast-enhanced CT using a fully automated deep learning volumetric hepatosplenic segmentation algorithm and unenhanced CT as the reference standard.

METHODS. A fully automated volumetric hepatosplenic segmentation algorithm using 3D convolutional neural networks was applied to unenhanced and contrast-enhanced series from a sample of 1204 healthy adults (mean age, 45.2 years; 726 women, 478 men) undergoing CT evaluation for renal donation. The mean volumetric attenuation was computed from all designated liver and spleen voxels. PDFF was estimated from unenhanced CT attenuation and served as the reference standard. Contrast-enhanced attenuations were evaluated for detecting PDFF thresholds of 5% (mild steatosis, 10% and 15% (moderate steatosis); PDFF less than 5% was considered normal.

RESULTS. Using unenhanced CT as reference, estimated PDFF was ≥ 5% (mild steatosis), ≥ 10%, and ≥ 15% (moderate steatosis) in 50.1% (n = 603), 12.5% (n = 151) and 4.8% (n = 58) of patients, respectively. ROC AUC values for predicting PDFF thresholds of 5%, 10%, and 15% using contrast-enhanced liver attenuation were 0.669, 0.854, and 0.962, respectively, and using contrast-enhanced liver-spleen attenuation difference were 0.662, 0.866, and 0.986, respectively. A total of 96.8% (90/93) of patients with contrast-enhanced liver attenuation less than 90 HU had steatosis (PDFF ≥ 5%); this threshold of less than 90 HU achieved sensitivity of 75.9% and specificity of 95.7% for moderate steatosis (PDFF ≥ 15%). Liver attenuation less than 100 HU achieved sensitivity of 34.0% and specificity of 94.2% for any steatosis (PDFF ≥ 5%). A total of 93.8% (30/32) of patients with contrast-enhanced liver-spleen attenuation difference 10 HU or less had moderate steatosis (PDFF ≥ 15%); a liver-spleen difference less than 5 HU achieved sensitivity of 91.4% and specificity of 95.0% for moderate steatosis. Liver-spleen difference less than 10 HU achieved sensitivity of 29.5% and specificity of 95.5% for any steatosis (PDFF ≥ 5%).

CONCLUSION. Contrast-enhanced volumetric hepatosplenic attenuation derived using a fully automated deep learning CT tool may allow objective categoric assessment of hepatic steatosis. Accuracy was better for moderate than mild steatosis. Further confirmation using different scanning protocols and vendors is warranted.

CLINICAL IMPACT. If these results are confirmed in independent patient samples, this automated approach could prove useful for both individualized and population-based steatosis assessment.

Nonalcoholic fatty liver disease (NAFLD) is a highly prevalent public health issue, with cardiovascular, metabolic, and liver-specific implications [1–3]. Although not a defining criterion, NAFLD is closely associated with the obesity and metabolic syndrome epidemics that are prevalent throughout the world [4–6]. A majority of American adults are now considered obese, and approximately half of all American adults may have some degree

[1]Department of Radiology, The University of Wisconsin School of Medicine & Public Health, E3/311 Clinical Science Center, 600 Highland Ave, Madison, WI 53792-3252. Address correspondence to P. J. Pickhardt (ppickhardt2@uwhealth.org).

[2]Department of Biomedical Engineering, School of Biomedical Engineering & Imaging Sciences, King's College London, St Thomas' Hospital, London, United Kingdom.

[3]Imaging Biomarkers and Computer-Aided Diagnosis Laboratory, Radiology and Imaging Sciences, National Institutes of Health Clinical Center, Bethesda, MD.

doi.org/10.2214/AJR.20.24415
AJR 2021; 217:359–367
ISSN-L 0361–803X/21/2172–359

of hepatic steatosis [7, 8]. Despite the growing importance of identifying steatosis, there is no reliable noninvasive, non-imaging-based clinical method for accurately quantifying or even categorizing the degree of steatosis. Liver biopsy for the sole purpose of assessing hepatic steatosis at histopathology is costly and invasive and generally provides only a subjective visual estimate of steatosis and may include sampling errors. From a population-based standpoint, noninvasive imaging methods for liver fat quantification would be advantageous.

MRI-based proton density fat fraction (PDFF) should be the preferred noninvasive reference standard for quantifying liver fat given its accuracy and whole-liver assessment [9]. Recent studies using different CT vendors showed the linear equivalence between MRI PDFF and unenhanced CT attenuation [10–12]. This equivalence allows CT to be used to quantify liver fat, especially that beyond normal or low levels. Furthermore, because abdominal CT is performed in clinical practice much more frequently than abdominal MRI, CT can serve as a surrogate for initial detection of steatosis [13]. For these reasons, unenhanced CT may represent a practical noninvasive reference standard for routine liver fat quantification, especially for population-based studies [14]. However, CT assessment of liver fat content after IV contrast administration remains much more challenging.

A fully automated algorithm for quantifying liver fat at unenhanced CT was recently validated in a large sample of patients without symptoms [8]. This volumetric deep learning tool was compared against the standard manual ROI approach [11, 15–17]. The tool automatically segments and analyzes both the liver and spleen. However, to realize the full potential of this automated tool for population-based opportunistic hepatic steatosis and NAFLD screening, the next challenge is to apply it to contrast-enhanced CT obtained in the portal venous phase or later. Although the direct linear relationship between CT attenuation and MRI-based PDFF no longer holds after IV contrast administration, patients may potentially be placed into PDFF categories (e.g., normal, mild, and moderate or greater steatosis) according to contrast-enhanced liver attenuation, with or without incorporating splenic attenuation. The purpose of this study was to evaluate liver steatosis categorization on contrast-enhanced CT using the fully automated deep learning volumetric hepatosplenic segmentation algorithm and unenhanced CT as the reference standard.

Methods

Study Sample

This retrospective study was approved by the institutional review board at the University of Wisconsin-Madison and was HIPAA-compliant; the requirement for written informed consent was waived. A total of 1250 consecutive adults who underwent multiphasic abdominal CT at a single academic medical center for the purpose of potential renal donation between February 2010 and January 2017 were initially included. After exclusion of 46 patients because of missing or corrupted CT image data (n = 39) or splenic absence (n = 7), the final study sample consisted of 1204 healthy adults with usable CT image data. Before automated CT-based assessment, patient information was anonymized.

HIGHLIGHTS

Key Finding

- *Using estimated MRI PDFF from unenhanced CT as reference, contrast-enhanced liver attenuation from a fully automated deep learning volumetric segmentation tool achieved ROC AUC of 0.962 for detecting moderate steatosis (PDFF ≥ 15%) and 75.9% sensitivity and 95.7% specificity at a contrast-enhanced CT threshold of less than 90 HU.*

Importance

- *Opportunistic detection of hepatic steatosis on abdominal CT performed for other indications may help address nonalcoholic fatty liver disease, a highly prevalent public health issue.*

CT Protocol

All individuals in the study sample underwent abdominal CT using a dedicated multiphasic protocol. All scans were performed on MDCT scanners predominately using a size-based protocol with 64 × 0.625 detector configuration, 120 kVp setting, modulated tube current, and a noise index ranging from 17.0 to 27.5. An unenhanced abdominal series was obtained extending from T12 to L4. A split-bolus IV contrast enhancement technique was used to achieve multiphase dynamic and excretory imaging. An initial injection consisted of 20 mL of nonionic contrast material (with 20 mL saline flush) 5 minutes before the dynamic multiphasic injection to opacify the upper collecting system. Dynamic multiphasic injection consisted of a split bolus of 30 mL contrast material (and 30 mL saline) at 3 mL/s for the arterial (vascular) phase, followed by 100 mL contrast material per 50 mL saline at 5 mL/s 20 seconds later for the late portal venous (parenchymal) phase. Arterial and parenchymal phase series were then obtained. The arterial phase was intended for renal vascular assessment and did not provide sufficient hepatic coverage for the present investigation. The arterial phase is also of less practical value for liver fat quantification given the phase's greater sensitivity to timing and hypervascularity of the spleen. Thus, this study used only the unenhanced and parenchymal contrast-enhanced phases for assessing the automated CT tool. Imaging series were originally reconstructed as 5-mm slices at 3-mm intervals, which were then retrospectively reformatted to 3-mm contiguous slices.

Automated Algorithm for Hepatosplenic Segmentation and Analysis

The methodology for automated hepatosplenic assessment has been previously described in detail [18]. A modified 3D convolutional neural network (U-Net) was used. Imaging data for training were obtained from a separate patient sample [19]. Data augmentation was performed using 3D rotation, crop, elastic deformation, the CycleGAN automatic image-to-image translation technique for the unenhanced images, and random flips. Training of the model used the National Institutes of Health (NIH) Bio-

wulf High Performance Computing cluster. The volumetric mean attenuation was computed for all designated liver voxels. The intrahepatic vasculature was included in the segmentation. A similar process was used for the spleen.

Liver Fat Quantification Reference Standard

The mean unenhanced CT liver attenuation obtained from the automated volumetric tool was converted to the MRI-based PDFF-equivalent fat fraction using the recently published formula [11],

$$\text{Fat fraction (\%)} = (-0.58 \times \text{CT attenuation in HU}) + 38.2.$$

This unenhanced CT hepatic fat fraction served as the reference standard to which the contrast-enhanced attenuation was compared. The linear relationship between CT hepatic fat fraction and PDFF equivalent has been verified in a prospective trial using a different CT vendor [12]. Although various steatosis categories according to PDFF have been used, a recent study suggests that 5% should serve as the preferred threshold for normal (< 5%) versus mild steatosis, and 15% as the preferred threshold between mild and moderate steatosis [20]. We adopted these fat fraction thresholds of 5% and 15%, and used 10% to signify the midway point between mild and moderate steatosis. Although the prevalence of fat fraction greater than 20% was expected to be low in a sample of healthy outpatients, we considered this to signify a relatively more severe degree of steatosis.

Statistical Analysis

Sensitivity, specificity, PPV, NPV, and ROC curves for PDFF thresholds of 5%, 10%, and 15% were calculated in Excel (Microsoft) spreadsheets. Starting from columns of unenhanced and contrast-enhanced liver attenuations, the unenhanced attenuations were first converted to MRI PDFF–equivalent fat fractions using the calibration formula cited earlier. Each case was then identified as positive or negative for steatosis according to the selected PDFF thresholds (5%, 10%, or 15%). For each threshold, true-positive, true-negative, false-positive, and false-negative results were determined to derive sensitivity, specificity, PPV, NPV, and ROC curves. The ROC AUC was derived by summing all 1204 elemental areas individually calculated using the trapezoid method [21]. The statistical significance of the difference between the AUCs for enhanced CT liver attenuation and enhanced CT liver-spleen attenuation difference at each PDFF threshold was evaluated using the method of Hanley and McNeil [22].

Results

The mean age (± SD) of the 1204 healthy adults was 45.2 ± 12.4 years. The sample included 478 men and 726 women. According to the unenhanced CT reference standard and the PDFF conversion formula, the corresponding PDFF indicated 5% or greater (mild) steatosis in 50.1% (603/1204), 10% or greater steatosis in 12.5% (151/1204), 15% or greater (moderate) steatosis in 4.8% (58/1204), and 20% or greater steatosis in 1.4% (17/1204).

The automated tool was successfully run and provided a measure in all 1204 cases. Figure 1 shows scatterplots for both contrast-enhanced liver attenuation and liver-spleen attenuation difference versus PDFF (derived from the unenhanced liver attenuation). Prediction performance improved with greater degrees of underlying hepatic steatosis. ROC AUC values for automated contrast-enhanced liver attenuation alone in predicting PDFF thresholds of 5%, 10%, and 15% were 0.669, 0.854, and 0.962, respectively (Fig. 2A). ROC AUC values for contrast-enhanced liver-spleen attenuation difference in predicting PDFF thresholds of 5%, 10%, and 15% were 0.662, 0.866, and 0.986, respectively (Fig. 2B). These ROC AUC values were not significantly different between the two measures (p = .66, .54, and .19, respectively).

Figure 3 depicts bar graphs of PDFF or steatosis categories for a variety of contrast-enhanced liver attenuation thresholds and ranges. A total of 96.8% (90/93) of patients with a contrast-enhanced liver attenuation less than 90 HU had PDFF 5% or greater (at least mild steatosis). A total of 96.8% (727/751) of patients with a contrast-enhanced liver attenuation greater than 110 HU had PDFF less than 10%. Table 1 provides more detailed performance data for predicting steatosis categories according to relevant contrast-enhanced liver attenuation thresholds. For example, to predict moderate steatosis (PDFF ≥ 15%), a contrast-enhanced threshold of less than 90 HU achieved sensitivity of 75.9%, specificity of 95.7%, PPV of 47.3%, and NPV of 98.7%. To predict moderate steatosis, increasing the CT threshold to 110 HU achieved higher sensitivity of 98.3% but it resulted in a decreased specificity of 65.5%, and decreasing the CT threshold to 80 HU achieved higher specificity of 99.2% and decreased sensitivity to 55.2%. To predict any degree of hepatic steatosis (PDFF ≥ 5%), a contrast-enhanced threshold less than 120 HU achieved a sensitivity of 64.7% and a specificity of 52.1%; less than 100 HU achieved sensitivity of 34.0% and specificity of 94.2%; and less than 80 HU achieved a sensitivity of 6.8% and specificity of 100.0%.

Figure 4 depicts bar graphs of PDFF or steatosis categories for a variety of contrast-enhanced liver-spleen attenuation difference thresholds and ranges. A total of 93.8% (30/32) of patients with a liver-spleen difference of 10 HU or less had PDFF of 15% or greater (at least moderate steatosis). A total of 100.0% (15/15) of patients with a liver-spleen attenuation difference of 20 HU or less had PDF 15% or greater. A total of 86.8% (178/205) of patients with a liver-spleen attenuation difference of less than 10 HU had PDFF of 5% or greater (at least mild steatosis). Table 2 provides more detailed performance data for predicting steatosis categories according to relevant contrast-enhanced liver-spleen attenuation difference thresholds. For example, to predict moderate steatosis (PDFF ≥ 15%), a contrast-enhanced liver-spleen attenuation difference threshold of less than 5 HU achieved sensitivity of 91.4%, specificity of 95.0%, PPV of 48.2%, and NPV of 99.5%. To predict any degree of hepatic steatosis (PDFF ≥ 5%), a contrast-enhanced liver-spleen attenuation difference of less than 10 HU achieved sensitivity of 29.5% and specificity of 95.5%, and less than 0 HU (i.e., liver attenuation less than that of the spleen) achieved sensitivity of 10.8% and specificity of 100.0%.

Discussion

Although it has been shown that liver fat content can be estimated on unenhanced CT scans using the linear conversion formula with MRI-based PDFF, quantification at contrast-enhanced CT remains elusive, owing to the complexities of hepatic contrast enhancement [10, 11]. Nonetheless, we found that categoric assignment of fat content according to contrast-enhanced CT is feasible,

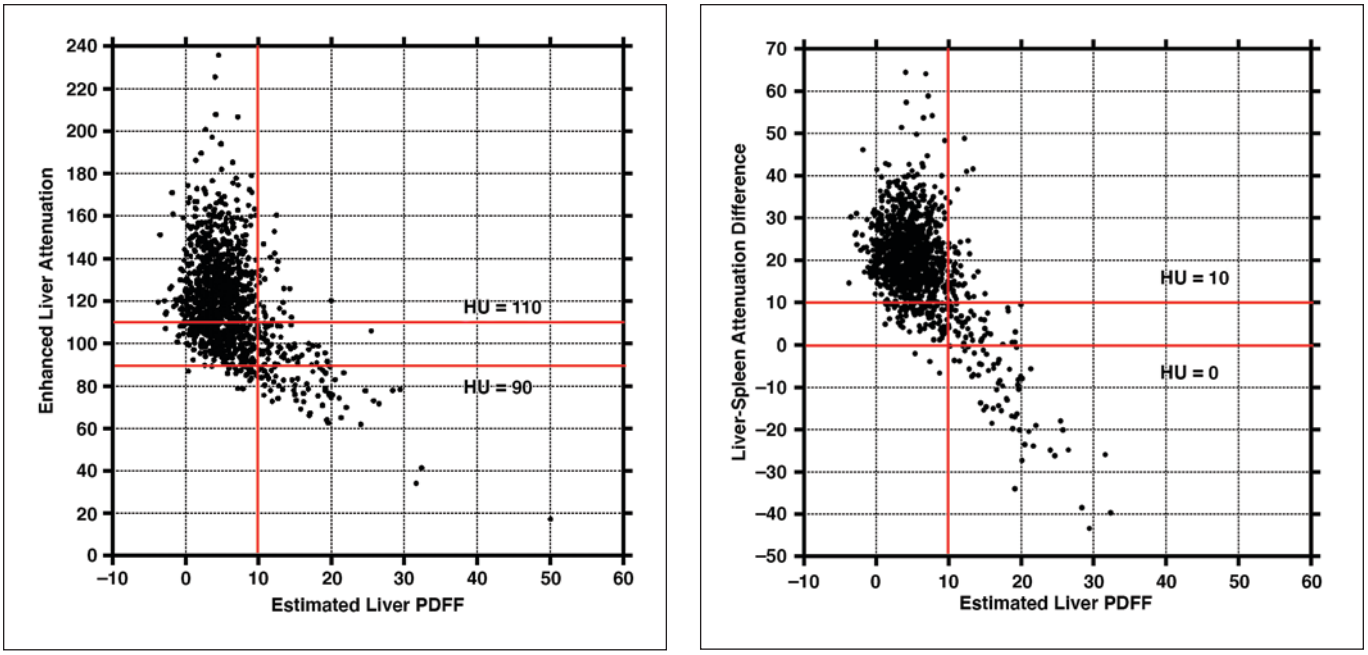

A B

Fig. 1—Scatterplots of contrast-enhanced CT showing attenuation versus estimated MRI-based proton density fat fraction (PDFF).
A and **B,** Scatterplots of liver attenuation (**A**) and liver-spleen attenuation difference (**B**) versus estimated PDFF according to unenhanced CT series. Plots are similar for two contrast-enhanced CT attenuation measures.

especially for at least moderate steatosis. Using the contrast-enhanced liver attenuation alone performed well and is more straightforward than including splenic attenuation. As such, our data do not clearly support the inclusion of splenic attenuation. Regardless, distinction between normal and mild steatosis (i.e., around the 5% PDFF threshold) remains a diagnostic challenge using contrast-enhanced CT attenuation with very low sensitivity. External validation of our findings in a variety of practice settings is still needed.

The ability to use unenhanced CT as the reference standard for liver fat content was advantageous. Put in context for routine practice, the unenhanced CT thresholds for any steatosis (PDFF ≥ 5%) and moderate steatosis (PDFF ≥ 15%) correspond to 57 HU and 40 HU, respectively, at 120 kVp tube potential. However, on clinical patient scans, the relationship between unenhanced CT attenuation and MRI PDFF weakens somewhat at lower levels of fat content (e.g., ≈ 5% PDFF) compared with performance in a phantom model [11, 12]. Earlier work also showed lower agreement between unenhanced CT and histopathology near the threshold between normal and mild steatosis [23]. This may help explain why contrast-enhanced CT performance in our study was poorer around the 5% PDFF threshold. Although splenic attenuation provides no additional value to liver attenuation for liver fat

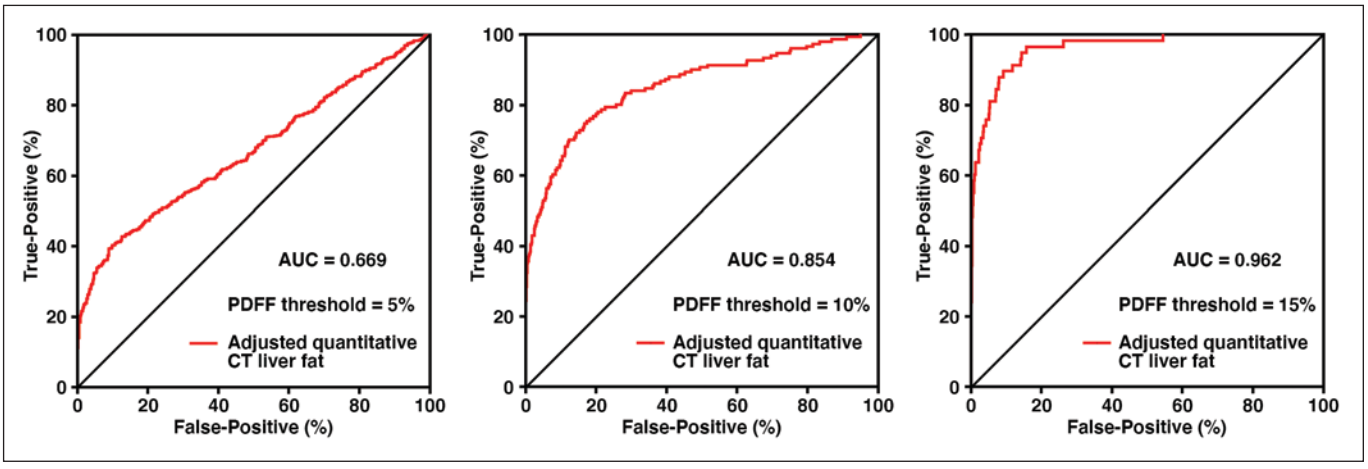

A

Fig. 2—ROC curves for predicting liver fat content from contrast-enhanced series.
A and **B,** ROC curves are shown for proton density fat fraction (PDFF)–equivalent thresholds of 5% (*left*), 10% (*middle*), and 15% (*right*) for enhanced liver attenuation (**A**) and liver-spleen attenuation difference (**B**). Corresponding AUC values are similar for each steatosis threshold. Performance improves for greater degrees of steatosis.

(Fig. 2 continues on next page)

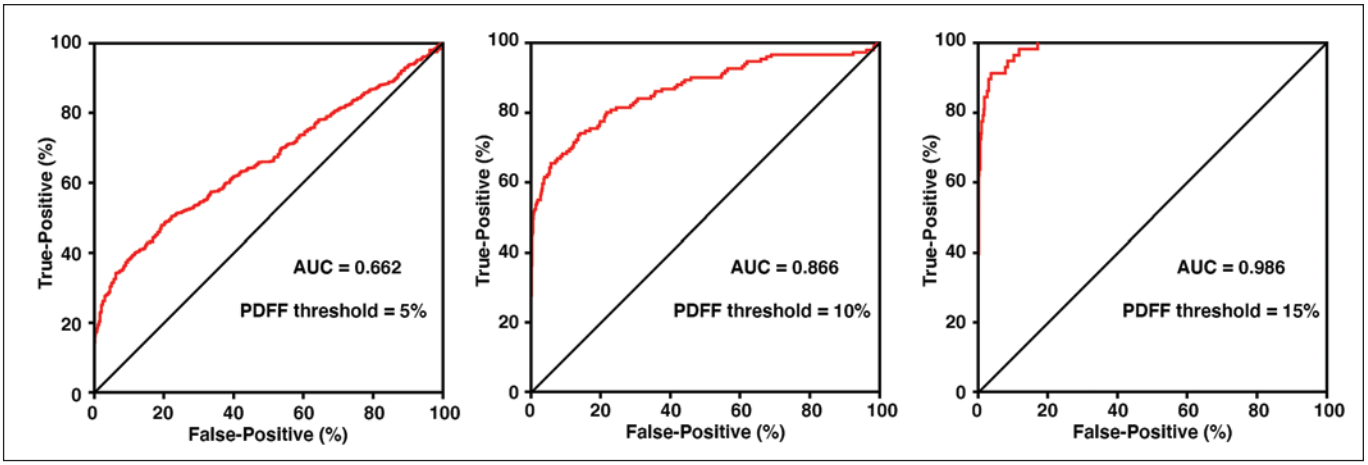

Fig. 2 (continued)—ROC curves for predicting liver fat content from contrast-enhanced series.
A and **B,** ROC curves are shown for proton density fat fraction (PDFF)–equivalent thresholds of 5% (*left*), 10% (*middle*), and 15% (*right*) for enhanced liver attenuation (**A**) and liver-spleen attenuation difference (**B**). Corresponding AUC values are similar for each steatosis threshold. Performance improves for greater degrees of steatosis.

quantification at unenhanced CT, it has shown variable utility after IV contrast enhancement expressed either as a ratio or difference with liver attenuation [16, 24–27].

Other investigators have also studied the ability of contrast-enhanced hepatosplenic attenuation to predict hepatic steatosis, typically with a manual ROI technique and a histopathologic reference standard [25–27]. As with our findings, the results are generally reported in categoric terms (e.g., normal versus mild or moderate steatosis) and not as a continuous percentage. One study found that a liver-spleen attenuation difference of –19 HU was the optimal cutoff for moderate steatosis, as defined by 30% or greater lipid droplets at histopathology [25]. However, another study showed that the absolute contrast-enhanced liver attenuation alone performed better than the liver attenuation normalized to spleen, either by an absolute difference or ratio [26]. Yet another study found that the rate and timing of contrast material injection significantly influenced the optimal liver-spleen attenuation threshold for diagnosing fatty liver [27].

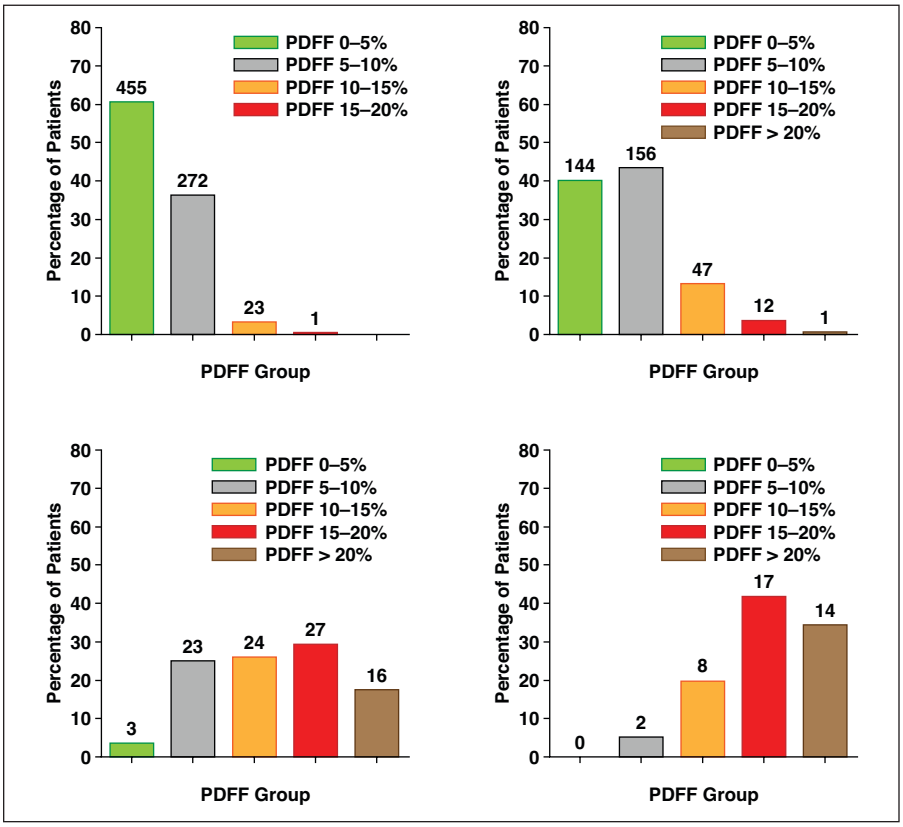

Fig. 3—Bar graphs depict liver fat content categories according to various thresholds of CT-estimated equivalent of proton density fat fraction (PDFF) estimated at CT and ranges for contrast-enhanced liver attenuation value, including attenuation greater than 110 HU (*top left*), 90–110 HU (*top right*), less than 90 HU (*bottom left*), and less than 80 HU (*bottom right*).

TABLE 1: Sensitivity, Specificity, PPV, and NPV for Various Thresholds of Contrast-Enhanced CT Liver Attenuation to Predict Liver Fat Content According to Proton Density Fat Fractions (PDFF) Equivalent

	PDFF ≥ 5%				PDFF ≥ 10%				PDFF ≥ 15%			
Attenuation (HU)[a]	Sens	Spec	PPV	NPV	Sens	Spec	PPV	NPV	Sens	Spec	PPV	NPV
80	6.8	100.0	100.0	51.7	25.8	99.8	95.1	90.4	55.2	99.2	78.1	97.8
90	14.9	99.5	96.8	53.8	44.4	97.5	72.0	92.4	75.9	95.7	47.3	98.7
95	22.7	98.3	93.2	55.9	56.3	94.1	57.8	93.8	87.9	91.6	34.7	99.3
100	34.0	94.2	85.4	58.7	70.2	87.3	44.2	95.3	96.6	83.9	23.3	99.8
105	42.0	87.4	76.9	60.0	77.5	79.9	35.6	96.1	96.6	76.2	17.0	99.8
110	50.9	75.7	67.8	60.6	84.1	69.0	28.0	96.8	98.3	65.5	12.6	99.9
115	58.2	64.6	62.2	60.6	88.1	59.1	23.6	97.2	98.3	55.8	10.1	99.8
120	64.7	52.1	57.5	59.5	90.7	48.5	20.2	97.3	98.3	45.8	8.4	99.8

Note—Values are percentages. Sens = sensitivity, Spec = specificity.
[a]Contrast-enhanced CT liver attenuation measured by automated volumetric deep learning tool.

Dual-energy CT (DECT) offers another potential solution to quantifying liver fat at contrast-enhanced CT. As with splenic attenuation assessment, DECT does not improve on unenhanced single-energy CT for liver fat quantification, except potentially in cases of superimposed iron overload or amiodarone therapy [10, 28–31]. However, in the setting of iodinated contrast material, a multimaterial decomposition approach has provided direct liver fat quantification in experimental studies [31, 32]. A more simplistic clinical DECT approach consists of deriving virtual unenhanced images that if closely matched to true unenhanced liver attenuation would provide fat quantification. In practice, however, the fidelity of virtual unenhanced image matching with the true unenhanced attenuation values can vary according to scanner vendor and model [33, 34].

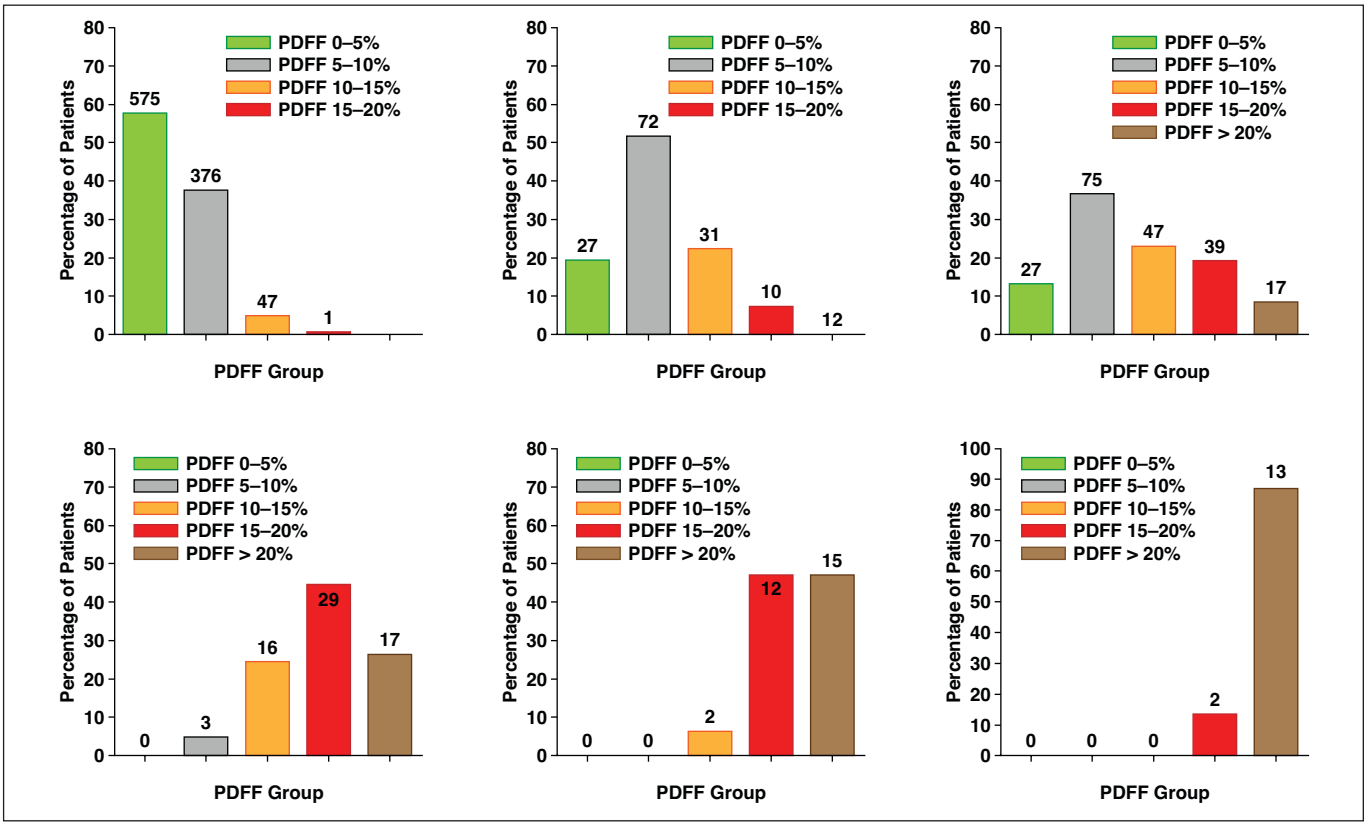

Fig. 4—Bar graphs depict liver fat content categories according to various thresholds of CT-estimated equivalent for proton density fat fraction (PDFF) estimated at CT and ranges for contrast-enhanced liver-spleen attenuation differences, including greater than 10 HU (*top left*), 0–10 HU (*top middle*), less than 10 HU (*top right*), less than 0 HU (*bottom left*), less than –10 HU (*bottom middle*), and less than –20 HU (*bottom right*).

TABLE 2: Sensitivity, Specificity, PPV, and NPV for Various Thresholds of Contrast-Enhanced CT Liver-Spleen Attenuation to Predict Liver Fat Content According to Proton Density Fat Fractions (PDFF) Equivalent

	PDFF ≥ 5%				PDFF ≥ 10%				PDFF ≥ 15%			
Attenuation (HU)[a]	Sens	Spec	PPV	NPV	Sens	Spec	PPV	NPV	Sens	Spec	PPV	NPV
–10	5.3	100.0	100.0	51.3	21.2	100.0	100.0	89.9	51.7	99.8	93.8	97.6
–5	8.0	100.0	100.0	52.0	31.1	99.9	97.9	91.0	70.7	99.4	85.4	98.5
0	10.8	100.0	100.0	52.8	41.1	99.7	95.4	92.2	79.3	98.3	70.8	99.0
5	17.6	99.3	96.4	54.6	55.0	97.4	75.5	93.8	91.4	95.0	48.2	99.5
10	29.5	95.5	86.8	57.5	68.2	90.3	50.2	95.2	98.3	87.1	27.8	99.9
15	45.1	82.2	71.8	59.9	80.8	75.6	32.2	96.5	100.0	72.0	15.3	100.0
20	63.2	57.4	59.8	60.9	90.1	52.4	21.4	97.4	100.0	49.5	9.1	100.0

Note—Values are percentages. Sens = sensitivity, Spec = specificity.
[a]Attenuation indicates contrast-enhanced CT liver-spleen absolute attenuation difference according to automated volumetric deep learning tool.

Whether as cause or effect, NAFLD is related to diabetes, obesity, hyperlipidemia, and metabolic syndrome [6]. The presence of at least mild steatosis (PDFF ≥ 5%) is remarkably common among adults in the United States and other industrialized populations and is a largely asymptomatic condition. The 50% prevalence of hepatic steatosis in our sample of healthy adults undergoing potential renal donation is similar to the prevalence of 52% in a recent study of more than 10,000 CT colonography examinations in healthy adults undergoing colorectal cancer screening [8]. That prior sample, which was older on average (mean age of 57 years vs 45 years for the current sample) did show a higher prevalence of moderate or severe steatosis (10% according to PDFF ≥ 14%) compared with our current sample (5% according to PDFF ≥ 15%). The prevalence of hepatic steatosis is lower, typically around 20–25%, when estimated using liver enzyme elevation or ultrasound rather than CT [35].

A recent study found a weak correlation between hepatic steatosis and body mass index (BMI), which implies that fatty liver cannot be reliably inferred from body habitus [8]. Although hepatic and visceral fat are not defining criteria for metabolic syndrome, they appear to provide valuable information beyond BMI and may ultimately provide an improved definition of metabolic syndrome [5–6]. Another recent study showed that automated CT-based assessment of hepatic steatosis was predictive of future adverse events, including major cardiovascular events and mortality [36]. Automated CT-based assessment of these key abdominal fat measures could be used for opportunistic NAFLD and metabolic syndrome screening, regardless of the reason for the scan.

Large volumes of abdominal CT examinations are performed each year, presenting an opportunity to screen for many conditions beyond the primary imaging indication [13]. In addition to providing an opportunity to evaluate hepatic steatosis, CT can also allow the noninvasive evaluation of the liver for fibrosis and hemochromatosis [15–17, 29, 37–41]. Beyond the liver and metabolic syndrome, other opportunistic screening situations include screening for osteoporosis and associated fractures, abdominal aortic calcification and aneurysm, sarcopenia, and cancer [42–46]. Many of these opportunistic tasks can be automated through artificial intelligence, which avoids the subjectivity and time constraints related to manual measurements [47].

We acknowledge limitations to this investigation. All scans were derived from a single academic institution using scanners from a single CT vendor. The contrast-enhanced phase used in this study was not a pure portal venous acquisition. However, the scanning protocol ensured adequate timing for liver parenchymal enhancement, whereas the portal venous phase can be obtained too early in some patients. Nonetheless, further external validation of this automated tool is warranted in diverse patient populations, with additional scanning protocols including a true portal venous phase, and with other CT vendors. Our reference standard for liver fat quantification was established using unenhanced CT, for which a previously validated formula was used to convert to an MRI-based PDFF equivalent. This approach may also warrant validation in a wider variety of practice settings. However, advantages over histopathologic correlation of using MRI-based PDFF, and by extension unenhanced CT, as a reference standard include its precision, objectivity, wider sampling, and noninvasiveness. Finally, inclusion of intrahepatic vessels in the automated liver segmentation may affect liver attenuation estimation. For unenhanced CT, this may partially explain the mean 2.7 attenuation difference between manual and automated techniques [8]. For contrast-enhanced CT, the impact of vessel inclusion should be greater with higher degrees of steatosis, given a more pronounced difference between enhanced vessel and parenchyma. Nonetheless, we believe the impact of vessel inclusion to be very small.

In conclusion, contrast-enhanced hepatic and splenic attenuation derived using a fully automated deep learning volumetric segmentation CT tool allowed adequate categoric assessment of hepatic steatosis, especially at higher PDFF levels. The contrast-enhanced liver attenuation alone performed reasonably well, potentially precluding the need for splenic attenuation consideration. This automated approach could prove useful for both individualized and population-based assessments for NAFLD if our findings are confirmed by other groups.

Acknowledgment

We thank NVIDIA for graphics processing unit card donation.

References

1. Lonardo A, Ballestri S, Marchesini G, Angulo P, Loria P. Nonalcoholic fatty liver disease: a precursor of the metabolic syndrome. *Dig Liver Dis* 2015; 47:181–190
2. Targher G, Byrne CD, Lonardo A, Zoppini G, Barbui C. Non-alcoholic fatty liver disease and risk of incident cardiovascular disease: a meta-analysis. *J Hepatol* 2016; 65:589–600
3. Wree A, Broderick L, Canbay A, Hoffman HM, Feldstein AE. From NAFLD to NASH to cirrhosis—new insights into disease mechanisms. *Nat Rev Gastroenterol Hepatol* 2013; 10:627–636
4. Neeland IJ, Ross R, Després JP, et al.; International Atherosclerosis Society; International Chair on Cardiometabolic Risk Working Group on Visceral Obesity. Visceral and ectopic fat, atherosclerosis, and cardiometabolic disease: a position statement. *Lancet Diabetes Endocrinol* 2019; 7:715–725
5. Pickhardt PJ, Jee Y, O'Connor SD, del Rio AM. Visceral adiposity and hepatic steatosis at abdominal CT: association with the metabolic syndrome. *AJR* 2012; 198:1100–1107
6. Pickhardt PJ, Graffy PM, Zea R, et al. Utilizing fully automated abdominal CT-based biomarkers for opportunistic screening for metabolic syndrome in adults without symptoms. *AJR* 2021; 216:85–92
7. Bellentani S. The epidemiology of non-alcoholic fatty liver disease. *Liver Int* 2017; 37(suppl 1):81–84
8. Graffy PM, Sandfort V, Summers RM, Pickhardt PJ. Automated liver fat quantification at nonenhanced abdominal CT for population-based steatosis assessment. *Radiology* 2019; 293:334–342
9. Reeder SB, Hu HH, Sirlin CB. Proton density fat-fraction: a standardized MR-based biomarker of tissue fat concentration. *J Magn Reson Imaging* 2012; 36:1011–1014
10. Kramer H, Pickhardt PJ, Kliewer MA, et al. Accuracy of liver fat quantification with advanced CT, MRI, and ultrasound techniques: prospective comparison with MR spectroscopy. *AJR* 2017; 208:92–100
11. Pickhardt PJ, Graffy PM, Reeder SB, Hernando D, Li K. Quantification of liver fat content with unenhanced MDCT: phantom and clinical correlation with MRI proton density fat fraction. *AJR* 2018; 211:[web]W151–W157
12. Guo Z, Blake GM, Li K, et al. Liver fat content measurement with quantitative CT validated against MRI proton density fat fraction: a prospective study of 400 healthy volunteers. *Radiology* 2020; 294:89–97
13. Moreno CC, Hemingway J, Johnson AC, Hughes DR, Mittal PK, Duszak R Jr. Changing abdominal imaging utilization patterns: perspectives from Medicare beneficiaries over two decades. *J Am Coll Radiol* 2016; 13:894–903
14. Starekova J, Hernando D, Pickhardt PJ, Reeder SB. Quantification of liver fat content with CT and MRI: state of the art. *Radiology* 2021 (in press)
15. Boyce CJ, Pickhardt PJ, Kim DH, et al. Hepatic steatosis (fatty liver disease) in asymptomatic adults identified by unenhanced low-dose CT. *AJR* 2010; 194:623–628
16. Hahn L, Reeder SB, Muñoz del Rio A, Pickhardt PJ. Longitudinal changes in liver fat content in asymptomatic adults: hepatic attenuation on unenhanced CT as an imaging biomarker for steatosis. *AJR* 2015; 205:1167–1172
17. Pickhardt PJ, Hahn L, Muñoz del Rio A, Park SH, Reeder SB, Said A. Natural history of hepatic steatosis: observed outcomes for subsequent liver and cardiovascular complications. *AJR* 2014; 202:752–758
18. Sandfort V, Yan K, Pickhardt PJ, Summers RM. Data augmentation using generative adversarial networks (CycleGAN) to improve generalizability in CT segmentation tasks. *Sci Rep* 2019; 9:16884
19. Simpson AL, Antonelli M, Bakas S, et al. A large annotated medical image dataset for the development and evaluation of segmentation algorithms. arXiv website. arxiv.org/abs/1902.09063. Published February 25, 2019. Accessed June 2, 2021
20. Cunha GM, Thai TT, Hamilton G, et al. Accuracy of common proton density fat fraction thresholds for magnitude- and complex-based chemical shift-encoded MRI for assessing hepatic steatosis in patients with obesity. *Abdom Radiol (NY)* 2020; 45:661–671
21. DeLong ER, DeLong DM, Clarke-Pearson DL. Comparing the areas under two or more correlated receiver operating characteristic curves: a nonparametric approach. *Biometrics* 1988; 44:837–845
22. Hanley JA, McNeil BJ. A method of comparing the areas under receiver operating characteristic curves derived from the same cases. *Radiology* 1983; 148:839–843
23. Lee SS, Park SH, Kim HJ, et al. Non-invasive assessment of hepatic steatosis: prospective comparison of the accuracy of imaging examinations. *J Hepatol* 2010; 52:579–585
24. Pickhardt PJ, Park SH, Hahn L, Lee SG, Bae KT, Yu ES. Specificity of unenhanced CT for non-invasive diagnosis of hepatic steatosis: implications for the investigation of the natural history of incidental steatosis. *Eur Radiol* 2012; 22:1075–1082
25. Kim DY, Park SH, Lee SS, et al. Contrast-enhanced computed tomography for the diagnosis of fatty liver: prospective study with same-day biopsy used as the reference standard. *Eur Radiol* 2010; 20:359–366
26. Kodama Y, Ng CS, Wu TT, et al. Comparison of CT methods for determining the fat content of the liver. *AJR* 2007; 188:1307–1312
27. Johnston RJ, Stamm ER, Lewin JM, Hendrick RE, Archer PG. Diagnosis of fatty infiltration of the liver on contrast enhanced CT: limitations of liver-minus-spleen attenuation difference measurements. *Abdom Imaging* 1998; 23:409–415
28. Artz NS, Hines CD, Brunner ST, et al. Quantification of hepatic steatosis with dual-energy computed tomography: comparison with tissue reference standards and quantitative magnetic resonance imaging in the ob/ob mouse. *Invest Radiol* 2012; 47:603–610
29. Lawrence EM, Pooler BD, Pickhardt PJ. Opportunistic screening for hereditary hemochromatosis with unenhanced CT: determination of an optimal liver attenuation threshold. *AJR* 2018; 211:1206–1211
30. Laukamp KR, Lennartz S, Hashmi A, et al. Iodine accumulation of the liver in patients treated with amiodarone can be unmasked using material decomposition from multiphase spectral-detector CT. *Sci Rep* 2020; 10:6994
31. Fischer MA, Gnannt R, Raptis D, et al. Quantification of liver fat in the presence of iron and iodine: an ex-vivo dual-energy CT study. *Invest Radiol* 2011; 46:351–358
32. Hyodo T, Hori M, Lamb P, et al. Multimaterial decomposition algorithm for the quantification of liver fat content by using fast-kilovolt-peak switching dual-energy CT: experimental validation. *Radiology* 2017; 282:381–389
33. Javadi S, Elsherif S, Bhosale P, et al. Quantitative attenuation accuracy of virtual non-enhanced imaging compared to that of true non-enhanced imaging on dual-source dual-energy CT. *Abdom Radiol (NY)* 2020; 45:1100–1109
34. Laukamp KR, Ho V, Obmann VC, et al. Virtual non-contrast for evaluation of liver parenchyma and vessels: results from 25 patients using multi-phase spectral-detector CT. *Acta Radiol* 2020; 61:1143–1152
35. Younossi Z, Anstee QM, Marietti M, et al. Global burden of NAFLD and NASH: trends, predictions, risk factors and prevention. *Nat Rev Gastroenterol Hepatol* 2018; 15:11–20
36. Pickhardt PJ, Graffy PM, Zea R, et al. Automated CT biomarkers for opportunistic prediction of future cardiovascular events and mortality in an asymptomatic screening population: a retrospective cohort study. *Lancet Digit Health* 2020; 2:E192–E200
37. Pickhardt PJ, Malecki K, Kloke J, Lubner MG. Accuracy of liver surface nodularity quantification on MDCT as a noninvasive biomarker for staging hepatic fibrosis. *AJR* 2016; 207:1194–1199

38. Pickhardt PJ, Malecki K, Hunt OF, et al. Hepatosplenic volumetric assessment at MDCT for staging liver fibrosis. *Eur Radiol* 2017; 27:3060–3068
39. Lubner MG, Jones D, Kloke J, Said A, Pickhardt PJ. CT texture analysis of the liver for assessing hepatic fibrosis in patients with hepatitis C virus. *Br J Radiol* 2019; 92:20180153
40. Lubner MG, Pickhardt PJ. Multidetector computed tomography for retrospective, noninvasive staging of liver fibrosis. *Gastroenterol Clin North Am* 2018; 47:569–584
41. Pickhardt PJ, Graffy PM, Said A, et al. Multiparametric CT for noninvasive staging of hepatitis C virus-related liver fibrosis: correlation with the histopathologic fibrosis score. *AJR* 2019; 212:547–553
42. Graffy PM, Liu J, Pickhardt PJ, Burns JE, Yao J, Summers RM. Deep learning-based muscle segmentation and quantification at abdominal CT: application to a longitudinal adult screening cohort for sarcopenia assessment. *Br J Radiol* 2019; 92:20190327
43. Jang S, Graffy PM, Ziemlewicz TJ, Lee SJ, Summers RM, Pickhardt PJ. Opportunistic osteoporosis screening at routine abdominal and thoracic CT: normative L1 trabecular attenuation values in more than 20000 adults. *Radiology* 2019; 291:360–367
44. O'Connor SD, Graffy PM, Zea R, Pickhardt PJ. Does nonenhanced CT-based quantification of abdominal aortic calcification outperform the Framingham risk score in predicting cardiovascular events in asymptomatic adults? *Radiology* 2019; 290:108–115
45. Pickhardt PJ, Lee SJ, Liu J, et al. Population-based opportunistic osteoporosis screening: validation of a fully automated CT tool for assessing longitudinal BMD changes. *Br J Radiol* 2019; 92:20180726
46. Pickhardt PJ, Kim DH, Meiners RJ, et al. Colorectal and extracolonic cancers detected at screening CT colonography in 10,286 asymptomatic adults. *Radiology* 2010; 255:83–88
47. Pickhardt PJ, Graffy PM, Lubner MG, Summers RM. Opportunistic screening at abdominal CT using automated biomarkers: adding value beyond the clinical indication. *RadioGraphics* 2021; 41:524–542

Editorial Comment on "Liver Steatosis Categorization on Contrast-Enhanced CT Using a Fully Automated Deep Learning Volumetric Segmentation Tool: Evaluation in 1204 Healthy Adults Using Unenhanced CT as a Reference Standard"

Nonalcoholic fatty liver disease (NAFLD) is becoming the leading cause of chronic liver disease in the United States and worldwide with approximately one-third of patients having progressive fibrosis [1]. Unlike those with other causes of chronic liver disease (with more clear risk factors, usually diagnosed on clinical grounds), patients with NAFLD have nonspecific and less distinct risk factors. Hence, imaging-based detection of hepatic steatosis has become one of the main pillars of diagnosis of NAFLD. Additionally, imaging often serendipitously reveals hepatic steatosis in unsuspected cases (referred to as opportunistic detection of steatosis) given the high prevalence of this disease, triggering clinical and laboratory workup [2]. MRI (specifically MRI-based proton density fat fraction) is established as the imaging modality with utmost accuracy for detection and quantification of hepatic steatosis, whereas sonography, although less accurate, is considered the first-line imaging in cases of clinically suspected NAFLD (given the lower cost and easier availability) [3]. Realistically, the main role of CT in NAFLD is for opportunistic diagnosis of hepatic steatosis in individual patients and for population-based studies, given the wider use of CT for a myriad of diseases. Therefore, gaining a better understanding of CT performance and setting better criteria for detection of hepatic steatosis remain of high importance. The currently used criteria for CT-based detection of moderate-to-severe hepatic steatosis calls for use of the unenhanced phase with 120-kVp conventional CT technique. Additional large-sample-size studies similar to this study are needed to enhance our knowledge of performance of CT for detection and categoric assessment of hepatic steatosis and to better understand the influence of phase of enhancement, tube voltage, CT technique (conventional versus spectral CT), and reconstruction algorithms.

Amir A. Borhani, MD
Northwestern University Feinberg School of Medicine
Chicago, IL
amir.borhani@northwestern.edu

The author declares that there are no disclosures relevant to the subject matter of this article.

doi.org/10.2214/AJR.20.24764

References

1. Calzadilla Bertot L, Adams LA. The natural course of non-alcoholic fatty liver disease. *Int J Mol Sci* 2016; 17:E774
2. Cheung A, Figueredo C, Rinella ME. Nonalcoholic fatty liver disease: identification and management of high-risk patients. *Am J Gastroenterol* 2019; 114:579–590
3. Reeder SB, Hu HH, Sirlin CB. Proton density fat-fraction: a standardized MR-based biomarker of tissue fat concentration. *J Magn Reson Imaging* 2012; 36:1011–1014